Microscopic Modes and Free Energies of 3-Phosphoinositide-Dependent Kinase-1 (PDK1) Binding with Celecoxib and Other Inhibitors

Mohamed Diwan M. AbdulHameed, Adel Hamza, and Chang-Guo Zhan*

Department of Pharmaceutical Sciences, College of Pharmacy, University of Kentucky, 725 Rose Street, Lexington, Kentucky 40536

Received: August 11, 2006; In Final Form: October 18, 2006

Celecoxib, also known as Celebrex (approved by FDA in 1998) and remembered as the fastest-selling drug in history, was used as a cyclooxygenase-2 (COX-2) selective inhibitor having both anti-inflammatory and anticancer activities. Most recent studies have revealed that the apoptotic activity of celecoxib (and its derivatives) is actually independent of the COX-2 inhibitory activity and that celecoxib also inhibits the kinase activity of 3-phosphoinositide-dependent protein kinase-1 (PDK1), suggesting that the well-known anticancer activity of celecoxib is not due to the inhibition of COX-2, but possibly is due to the inhibition of PDK1. It is highly desirable to develop new celecoxib derivatives as PDK1-specifc inhibitors to avoid the side effects of COX-2 inhibitors. To understand how PDK1 binds with celecoxib and its derivatives, we have performed extensive molecular docking and combined molecular dynamics (MD) simulations and molecular mechanics/Poisson−Boltzmann surface area (MM−PBSA) binding free energy calculations on eight representative PDK1 inhibitors, leading to the finding of a new, more favorable binding mode which is remarkably different from the previously proposed binding mode. Based on the determined most stable binding structures, the calculated binding free energies are all in good agreement with the corresponding experimental data, and the biological activity data available for celecoxib and its derivatives can be better interpreted. The obtained new insights, concerning both the binding mode and computational protocol, will be valuable not only for future rational design of novel, more potent PDK1-specific inhibitors as promising anticancer therapeutics, but also for rational design of drugs targeting other proteins.

Introduction

Protein kinases are known to be critical components of cellular signal transduction cascades.[1] In cancer cells, the kinase signaling pathways are often altered, resulting in uncontrolled growth and increased capability to invade surrounding tissue.[2] An altered or constitutively activated phosphoinositide-3-kinase (PI3K) pathway is reported in many human cancers.[3−5] Such an aberrant PI3K pathway is implicated in tumor development and progression and also in the tumor's response to cancer treatment.[6] 3-Phosphoinositide-dependent protein kinase-1 (PDK1) is a pivotal kinase for the PI3K pathway[7] and is an attractive target for anticancer therapeutics.[8] PDK1 is a serine/threonine kinase[9] and possesses an N-terminal kinase domain and C-terminal pleckstrin homology (PH) domain.[10,11] PDK1 is noted as the master regulator of the c*A*MP-dependent, c*G*MP-dependent, protein kinase *C* (AGC) kinase family.[12] It is known to activate at least 23 downstream AGC kinases.[13] These include protein kinase B (PKB, also known as Akt),[14,15] p70 ribosomal S6 kinase (S6K),[16] serum- and glucocorticoid-induced protein kinase (SGK),[17]and protein kinase C (PKC) isoforms.[18,19] The tumor suppressor, phosphatase, and tensin homologue deleted on chromosome Ten (PTEN), acts as the phosphatidylinositol 3-phosphatase[20] and thus down regulates the PDK1-mediated growth and signaling pathway. Mutations in PTEN resulting in elevated levels of phosphotidylinositol-3,4,5-triphosphate (PtdIns-(3,4,5)P_3) was reported in many human cancers, and in such cases inhibition of PDK1 is expected to mimic the tumor-suppressing activity of PTEN.[21] Moreover, most of the downstream proteins of PDK1 are also implicated in cancers.[7,22−25] As PDK1 is the master regulator of such AGC kinases, it is in a unique position to control all these proteins.

Accumulating pharmacologic and genetic evidence support the potential role of PDK1 as a promising anticancer target.[26−31] Many recent studies of PDK1 have been focused on the discovery and development of small molecule inhibitors of PDK1.[32−36] One of the interesting types of PDK1 inhibitors is celecoxib and its derivatives, because celecoxib has been a well-known FDA-approved drug in the market since 1998. Celecoxib (which is also known as Celebrex) is remembered as the fastest-selling drug in history.[37] It is known as a cyclooxygenase-2 (COX-2) selective inhibitor used as a nonsteroidal anti-inflammatory drug (NSAID). The success of celecoxib in the market is unprecedented. However, stomach and intestinal ulcers can occur with the use of celecoxib, although the incidence is less than with other NSAIDs in short-term studies.[38] Celecoxib can also be used for cancer prevention and treatment, which has become a very hot topic in the field of cancer research.[39−47] Interestingly, recent studies have shown that celecoxib has apoptotic effect independent of COX-2 inhibitory activity,[33] implying that the well-known anticancer activity of celecoxib is not due to the inhibition of COX-2. Further, a systematic structure−activity relationship (SAR) study was performed to identify the functional groups essential for apoptotic activity of celecoxib and similar compounds.[48] Another study has shown that celecoxib inhibits PDK1 kinase activity.[49] Zhu et al.[32] demonstrated that a series of celecoxib derivatives, through

* Corresponding author. Telephone: (859) 323-3943. Fax: (859) 323-3575. E-mail: zhan@uky.edu.

10.1021/jp065207e CCC: $33.50
Published on Web 12/01/2006

certain modification of the aryl group and other groups of celecoxib, are more potent PDK1 inhibitors that have the desired anticancer activity, but these celecoxib derivatives do not inhibit COX-2. Without inhibiting COX-2, these compounds are not expected to have the common side effects (such as the stomach and intestinal ulcers) of the COX-2 inhibitors. Further structural modifications of celecoxib could eventually lead to more potent PDK1 inhibitors as potentially more efficient anticancer drugs that do not have the side effects of celecoxib. According to Zhu et al.,[32] celecoxib has an IC_{50} value of 48 μM, whereas a series of celecoxib derivatives have IC_{50} values in the low micromolar range, for inhibiting PDK1 kinase activity.

To further develop a novel derivative of celecoxib with a lower IC_{50} value for PDK1, one first needs to understand how celecoxib and its known derivatives bind with PDK1. X-ray crystal structures are available for PDK1 binding with other PDK1 inhibitors in the active site.[36,50−52] The adenosine triphosphate (ATP) binding region in PDK1 is located in the hinge region between the N- and C-terminal lobes.[50] Based on the interaction of ATP, the ATP binding site in kinase is usually divided into the adenine region, sugar region, and phosphate region.[53] In PDK1, as in other kinases, the adenine region consists of hydrophobic residues and the adenine moiety also forms the conserved hydrogen bonds with the backbone of the hinge region.[50] The sugar region is hydrophilic and consists of acidic residues. The phosphate region is a solvent-exposed area.[54]

By using the available X-ray crystal structures, Zhu et al.[32] further proposed a microscopic binding mode for PDK1 binding with celecoxib and its derivatives based on some molecular docking tests with the compounds. Molecular docking methods are now being routinely used to predict protein−ligand binding modes.[55] Some important shortcomings of the currently used docking programs are associated with the difficulty of reliably accounting for the solvation/desolvation effects on and entropic contributions to the protein−ligand binding.[56] Obviously, it is crucial to know whether the proposed microscopic binding mode is reasonable for future rational drug design targeting PDK1. A reasonable microscopic binding mode for PDK1 binding with celecoxib and its derivatives could guide the rational design of significantly more potent PDK1 inhibitors. Hence, in further considering the limit of traditional molecular docking methods, we decided to reexamine all of the possible microscopic binding modes for PDK1 binding with celecoxib and its derivatives (Figure 1), along with some other known PDK1 inhibitors (Figure 2) whose structures of binding with PDK1 have been revealed by X-ray diffraction, by using more sophisticated computational modeling techniques, including molecular dynamics (MD) simulations and molecular mechanics/Poisson−Boltzmann surface area (MM−PBSA) calculations,[56] in addition to the molecular docking.

The molecular docking followed by MD simulations and MM−PBSA binding free energy calculations has allowed us to examine various possible microscopic binding modes for a given ligand with PDK1 and to theoretically determine the most favorable binding mode, i.e., the one with the lowest binding free energy. Thus, we have identified a new, more favorable binding mode for PDK1 binding with celecoxib and its derivatives. Based on the new binding mode, one can better understand the available SAR data and that the calculated binding free energies are all in good agreement with available experimental activity data, providing valuable new insights for future rational design of more potent PDK1 inhibitors.

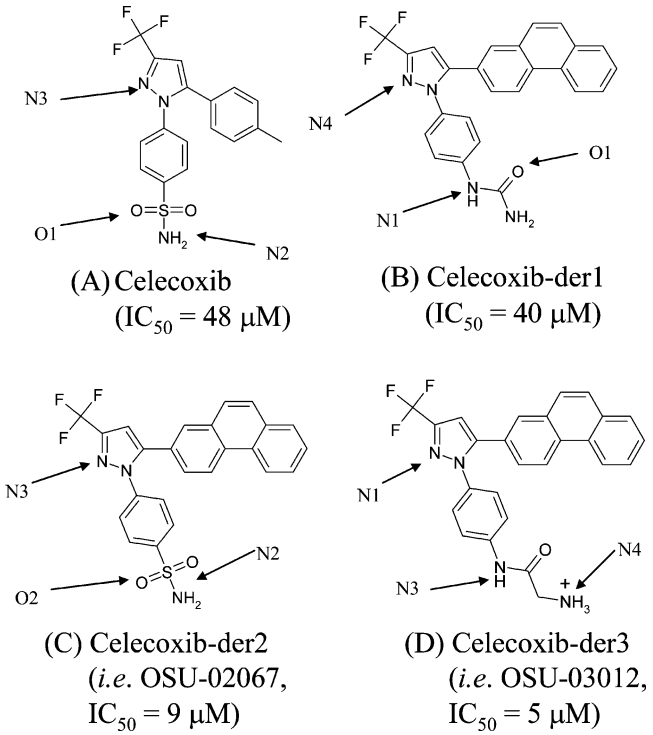

Figure 1. Molecular structures of celecoxib and its representative derivatives.

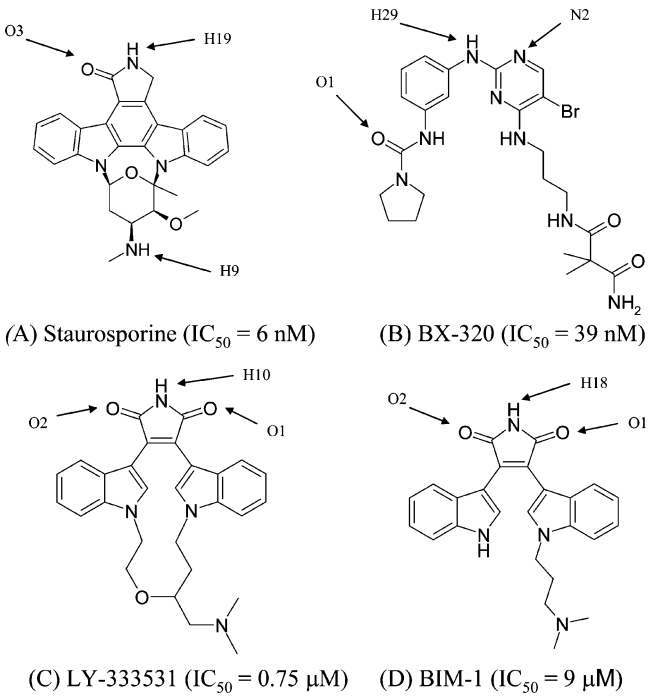

Figure 2. Molecular structures of staurosporine, BX-320, LY-333531, and BIM-1.

Computational Methods

General Computational Strategy. Due to the difficulty of accurately accounting for the solvation/desolvation effects on and entropic contributions to the binding free energy during molecular docking process,[56] the currently used docking scoring functions are not expected to consistently provide accurate predictions of the protein−ligand binding free energies for all of the protein−ligand binding systems. In addition, it is also difficult to account for the effects of protein dynamics on the microscopic binding during the simple docking process. Nev-

ertheless, the protein−ligand binding structures obtained from molecular docking can be considered as reasonable starting structures for molecular dynamics (MD) simulations in water that can more reasonably account for the solvation effects and the dynamics of the protein−ligand binding. The MD simulations allow us to obtain a dynamically stable protein−ligand binding mode associated with a stable MD trajectory. Further, the MD simulations are followed by the MM−PBSA calculations accounting for the contributions of the gas phase interactions, bulk solvent, and entropy to the binding free energies. When a ligand has multiple possible modes of binding with a protein, the relative binding free energies obtained from the MM−PBSA calculations can be used to determine the most favorable binding mode. The MD simulations followed by MM−PBSA calculations have been used to accurately predict the protein−protein and protein−ligand binding free energies for other systems.[57,58] Hence, the present work was based on a combined use of molecular docking, MD simulation, and MM−PBSA calculation.

Molecular Docking. A few X-ray crystal structures are available for PDK1 binding with inhibitors in the Protein Databank (PDB).[59] The starting protein structure used for our molecular docking is the X-ray crystal structure of ATP-bound PDK1 (PDB code: 2BIY),[13] as this structure is more complete compared with other X-ray crystal structures of PDK1. The missing side chain atoms of residues Gln73, Arg75, Glu153, Lys228, Arg238, Lys304, Glu343, Glu348, and Lys357 were modeled using the Sybyl 7.0 program.[60]

Molecular docking was carried out by using two different docking programs in order to obtain different initial binding structures for MD simulations. One is the FlexX module of the Tripos software.[61] FlexX uses an incremental docking algorithm called "pose clustering".[62] In this program, the ligand molecule is split into fragments and the core fragment is first placed according to a given scoring function.[62] The molecule is built up using the tree search, which performs the conformational search of the ligand and calculates its binding score.[62] Only the best conformation was built upon, and the others were discarded. The receptor description file for our docking with the FlexX module was built upon using the PDK1 structure,[52] and the residues within 5 Å around the ligand were defined as the active site. The docking was performed for four representative ligands, i.e., celecoxib and its three representative derivatives depicted in Figure 1, with different IC_{50} values for PDK1. The molecular structures of these ligands were drawn and energy-minimized by using the Sybyl 7.0 program with the Tripos force field.[63] For docking with each ligand, 30 poses were saved for further examination before the best possible poses were chosen based on the docking scores.

The other program used in our molecular docking is DOCK,[64−66] which uses an incremental construction algorithm for flexible docking.[67] We also used the DOCK program because a previously reported binding mode[32] could not be obtained from the molecular docking using the FlexX for some protein−ligand binding systems. The DOCK program was used only in these special cases. The ligand orientations were scored through the use of a force-field-based energy scoring function, and the top-scoring binding structure was selected. Both the FlexX and DOCK programs use an incremental docking algorithm for flexible docking of ligands. The major difference is that whereas the FlexX program uses an empirical scoring function based on the work of Bohm[68] and Klebe,[69] the DOCK program uses a grid-based energy scoring function.[70] The files of protein and ligands required for using the DOCK 5.2 program were prepared by using Sybyl 7.0. The active site spheres were prepared using the SPHGEN program.[71] The spheres were selected such that they covered the entire ligand-binding region. These spheres served to orient ligands in the active site.[72] Grid calculations were carried out by using 0.3 Å grid spacing.

Molecular Dynamics. The possible protein−ligand binding complexes obtained from the molecular docking with the ligands depicted in Figure 1 were used as the initial structures for MD simulations. We also examined other four ligands that have X-ray crystal structures available for their binding with PDK1, i.e., staurosporine (PDB code: 1OKY),[52] BX-320 (PDB code: 1Z5M),[36] LY-333531 (PDB code: 1UU8),[51] and BIM-1 (PDB code: 1UU3),[51] and carried out MD simulations on these four protein−ligand complexes. Residues 230−241 were missing in these structures. To complete the protein structures for these four complexes, each of these four incomplete X-ray crystal structures was superimposed with the complete protein structure constructed from the structure in 2BIY. Thus we obtained the complete protein structure binding with staurosporine, BX-320, LY-333531, and BIM-1. These complete complex structures were also used as the initial structures for MD simulations.

The general procedure for carrying out the MD simulations in water is essentially the same as that used in our previously reported computational studies.[72−74] Briefly, the MD simulations were performed using the Sander module of the Amber 8 program.[75] The partial atomic charges for the ligand atoms were calculated using the RESP protocol[76] after electrostatic potential calculations at the Hartree−Fock (HF) level with 6-31G* basis set using the Gaussian 03 program.[77] The Merz−Singh−Kollman scheme implemented in the program was used to select the surface points for evaluating the electrostatic potential and performing the charge fitting. Each PDK1−ligand binding complex was neutralized by adding counterions (three Cl^- ions) and was solvated in a rectangular box of TIP3P water molecules[78] with a minimum solute wall distance of 10 Å. The solvated systems were carefully equilibrated and fully energy-minimized. These systems were gradually heated from $T = 10$ K to $T = 298.15$ K in 35 ps before a production MD simulation run for 1 ns, or longer, until a stable MD trajectory was obtained for each of the simulated systems. The time step used for the MD simulations was 2 fs. Periodic boundary conditions in the NPT ensemble at $T = 298.15$ K with Berendsen temperature coupling[79] and $P = 1$ atm with isotropic molecule-based scaling[77] were applied. The SHAKE algorithm[80] was used to fix all covalent bonds containing hydrogen atoms. The non-bonded pair list was updated every 10 steps. The particle mesh Ewald (PME) method[81] was used to treat long-range electrostatic interactions. Restrain was placed on the C-α backbone atoms during the MD run. A residue-based cutoff of 12 Å was utilized for the noncovalent interactions. The time-dependent geometric parameters were carefully examined to make sure that we obtained a stable MD trajectory for each simulated protein−ligand binding system. The coordinates of the simulated system were collected every 1 ps during the simulation. The equally distributed 100 snapshots of the simulated structure within the stable MD trajectory were used to perform the MM−PBSA calculations (see below).

Binding Free Energy Calculation. The binding free energies were calculated by using the molecular mechanics/Poisson−Boltzmann surface area (MM−PBSA) free energy calculation method.[56] In the MM−PBSA method, the free energy of the receptor/protein−inhibitor binding, ΔG_{bind}, is obtained from the difference between the free energies of the receptor/protein−ligand complex (G_{cpx}) and the unbound receptor/protein (G_{rec})

and ligand (G_{lig}) as follows:

$$\Delta G_{bind} = G_{cpx} - G_{rec} - G_{lig} \quad (1)$$

The binding free energy (ΔG_{bind}) was evaluated as a sum of the changes in the molecular mechanical (MM) gas-phase binding energy (ΔE_{MM}), solvation free energy (ΔG_{sol}), and entropic contribution ($-T\Delta S$):

$$\Delta G_{bind} = \Delta E_{bind} - T\Delta S \quad (2)$$

$$\Delta E_{bind} = \Delta E_{MM} + \Delta G_{sol} \quad (3)$$

$$\Delta E_{MM} = \Delta E_{ele} + \Delta E_{vdw} \quad (4)$$

$$\Delta G_{sol} = \Delta G_{PB} + \Delta G_{np} \quad (5)$$

$$\Delta G_{np} = \gamma(\mathrm{SASA}) + \beta \quad (6)$$

The MM binding energies were calculated with the ANAL module of the Amber8 program. Electrostatic solvation free energy was calculated by the finite-difference solution to the Poisson−Boltzmann equation (ΔG_{PB}) as implemented in the Delphi program.[82,83] Used in the solvation calculation was a grid spacing of 0.5 Å, 80%-filled grid box, an exterior dielectric constant of 80, and an interior dielectric constant of 1. Parse radius[84] and Amber charge[85] were used in the Delphi calculations. The radius used for the solvent probe was 1.4 Å. The MSMS program[86] was used to calculate the SASA for the estimation of the nonpolar solvation energy (ΔG_{np}) using eq 6 with default parameters, i.e., $\gamma = 0.005\,42$ kcal/Å^2 and $\beta = 0.92$ kcal/mol. Further, the entropic contribution, $-T\Delta S$, to the binding free energy was also calculated at $T = 298.15$ K by using the NMODE module of the Amber8 program which is based on a combination of the standard classical statistical formulas[87] and normal-mode analysis.[88]

The final ΔE_{MM} and ΔG_{sol} values for each protein−ligand binding mode were taken as the averages of the respective ΔE_{MM} and ΔG_{sol} values calculated for the 100 snapshots. For these energetic calculations, the ligand and the receptor were studied using the snapshots from the complex simulation (without performing further energy minimization); the water molecules and counterions were stripped away before MM−PBSA analysis. To evaluate $-T\Delta S$, a full energy minimization was first performed on each species (receptor, ligand, or complex) prior to the normal-mode analysis. As the full energy minimization and normal-mode analysis are much more time-consuming than the single-point energy calculations, we evaluated the $-T\Delta S$ values for only 10 of the above 100 snapshots (i.e., one from each 10 of the above 100 snapshots). The final $-T\Delta S$ value for each protein−ligand binding mode was taken as the average of the $-T\Delta S$ values calculated for the 10 snapshots.

Most of the MD simulations were performed on a supercomputer (Superdome, with 256 shared-memory processors for parallel computing) at the University of Kentucky Center for Computational Sciences. The other computations were carried out on SGI Fuel workstations and a 34-processor IBM x335 Linux cluster in our own laboratory.

Results and Discussion

Binding with Staurosporine, BX-320, LY-333531, and BIM-1. X-ray crystal structures have been reported for PDK1 binding with some PDK1 inhibitors, including staurosporine,

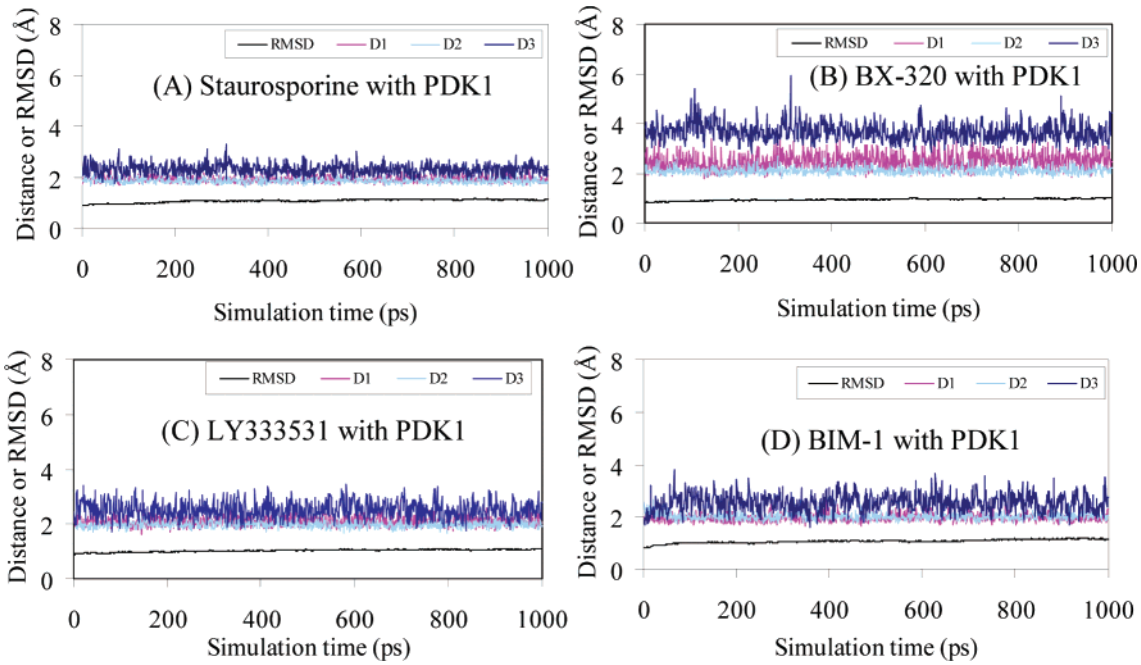

Figure 3. Plots of MD-simulated internuclear distances versus simulation time for PDK1 binding with staurosporine, BX-320, LY-333531, and BIM-1 (see Figure 2 for the structures and the positions of atoms referred to here). (A) Staurosporine: D1 refers to the distance between O3 atom of staurosporine and the NH hydrogen of Ala162 backbone, D2 is the distance between H19 atom of staurosporine and the carbonyl oxygen of Ser160 backbone, and D3 is the distance between H9 atom of staurosporine and the carbonyl oxygen of Glu209 backbone. (B) BX-320: D1 refers to the distance between H29 atom of BX-320 and the carbonyl oxygen of Ala162 backbone, D2 is the distance between N2 atom of BX-320 and the NH hydrogen of Ala162 backbone, and D3 is the distance between O1 atom of BX-320 and the NH nitrogen atom of Glu166 backbone. (C) LY-333531: D1 refers to the distance between O2 atom of LY-333531 and the NH hydrogen of Ala162 backbone, D2 is the distance between H10 atom of LY-333531 and the carbonyl oxygen of Ser160 backbone, and D3 is the distance between O1 atom of LY-333531 and the hydroxyl hydrogen of Thr222 side chain. (D) BIM-1: D1 refers to the distance between O2 atom of BIM-1 and the NH hydrogen of Ala162 backbone, D2 is the distance between H18 atom of BIM-1 and the oxygen atom of Ser160 backbone carbonyl group, and D3 is the distance between O1 atom of BIM-1 and the hydroxyl hydrogen of Thr222 side chain.

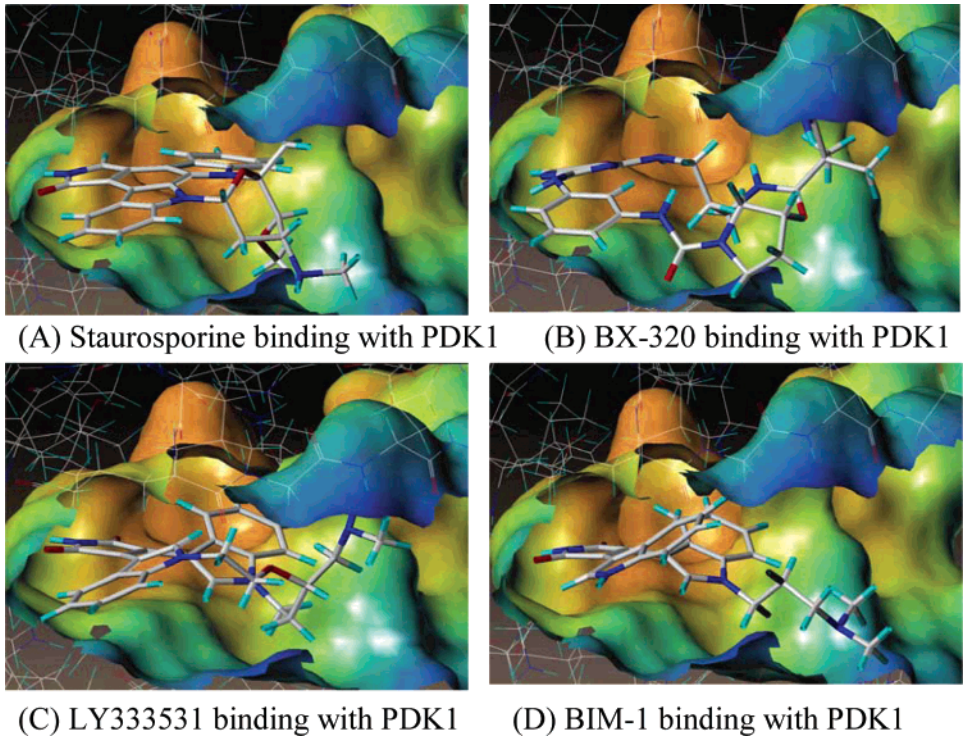

Figure 4. MD-simulated structures of PDK1 binding with (A) staurosporine, (B) BX-320, (C) LY-333531, and (D) BIM-1.

BX-320, LY-333531, and BIM-1 depicted in Figure 2. Staurosporine and BIM-1 are two of the most potent inhibitors of PDK1 known so far, but they are not PDK1-specific and can also potently inhibit many other kinases. Through MD simulations and MM−PBSA calculations on PDK1 binding with these four inhibitors whose binding modes have been known in the X-ray crystal structures, we wanted to know whether the computational protocol used in this study, i.e., MD simulations followed by MM−PBSA calculations, can reasonably predict the PDK1−ligand binding free energy for a given binding mode.

The MD simulation for each of the PDK1−ligand binding structures was quickly stabilized, because there was no any significant structural change during the simulation (see Figure 3 for the MD trajectories). The MD-simulated PDK1−ligand binding structures (Figure 4) are all essentially the same as the corresponding X-ray crystal structures. We did not note any significant difference between the MD-simulated structures and the corresponding X-ray crystal structures. The energetic results obtained from the MM−PBSA calculations for these binding structures are summarized in Table 1, in comparison with available experimental data. As seen in Table 1, the calculated binding free energies (ΔG_{bind}) are all in good agreement with the corresponding experimental ΔG_{bind} values (derived from the experimental IC_{50} values reported in literature): the average absolute deviation is ~1.2 kcal/mol. More importantly, the qualitative order of the calculated ΔG_{bind} values is completely consistent with that of the experimental ΔG_{bind} values. The reasonable agreement between the calculated and experimental binding free energies suggests that the computational protocol is adequate for predicting PDK1 binding with its ligands.

Binding with Celecoxib and Its Derivatives. To understand how PDK1 binds with celecoxib and its derivatives, we considered four representative compounds (depicted in Figure 1) whose experimental IC_{50} values for inhibiting PDK1 kinase activity range from 48 μM to 5 μM. The molecular docking revealed two quite different possible binding modes for each of these compounds binding with PDK1, and the scores are given in Table 2. For all the compounds FlexX gave a new binding mode, and for celecoxib-der3 the FlexX result showed that the new binding mode has a better score than the previous binding mode. DOCK results showed only the mode which is similar to that proposed by Zhu et al.[32] Further MD simulations led to a stable MD trajectory, as seen in Figure 5 (and additional figures provided in the Supporting Information), for each of the binding modes (Figures 6−9). Thus, we could not simply judge which binding mode is more reasonable without further evaluating the relative binding free energies.

Based on the molecular docking followed by the MD simulations, one of the two possible binding modes (see modes "B" depicted in Figures 6−9) is similar to that proposed by

TABLE 1: Binding Free Energies (kcal/mol) Calculated at $T = 298.15$ K and $P = 1$ atm for PDK1 Binding with Representative Inhibitors in Comparison with the Corresponding Experimental Data

	calcd[a]				
inhibitor	ΔE_{MM}	ΔG_{sol}	$-T\Delta S$	ΔG_{bind}	exptl[b] ΔG_{bind}
staurosporine	−93.8 (1.4)	60.3 (1.3)	21.7 (2.5)	−11.8 (1.9)	−11.2
BX-320	−127.5 (2.1)	97.3 (2.2)	18.7 (1.9)	−11.5 (2.1)	−10.1
LY-333531	−107.7 (1.4)	77.4 (1.6)	20.1 (1.9)	−10.2 (1.8)	−8.4
BIM-1	−82.8 (1.4)	59.0 (1.8)	16.1 (2.4)	−7.7 (2.1)	−6.9

[a] The MM−PBSA calculations were performed on 100 snapshots along a stable MD trajectory for each PDK1−inhibitor binding complex. The results given in the table are the average values calculated for the 100 snapshots. [b] Experimental binding free energies were calculated from the experimental IC_{50} values reported in refs 36, 51, and 52 via $\Delta G_{bind} = RT \ln K_d \approx RT \ln IC_{50}$.

TABLE 2: Binding Free Energies (kcal/mol) Calculated at $T = 298.15$ K and $P = 1$ atm for PDK1 Binding with Celecoxib and its Derivatives (der1, der2, and der3) in Comparison with the Corresponding Experimental Data[a]

			MM−PBSA[e]				
compound	binding mode	docking scoring[d]	ΔE_{MM}	ΔG_{sol}	$-T\Delta S$	ΔG_{bind}	exptl.[f] ΔG_{bind}
celecoxib	this work[b]	−3.1	−56.5 (1.7)	40.1 (1.6)	11.3 (0.2)	−5.1 (1.1)	−5.9
	Zhu et al.[c]	(−43.8)	−59.1 (1.4)	48.5 (1.6)	11.0 (1.9)	0.4 (1.6)	
celecoxib-der1	this work[b]	−4.9	−71.2 (2.0)	54.8 (2.0)	11.9 (1.2)	−4.5 (1.6)	−6.0
	Zhu et al.[c]	(−47.9)	−61.0 (3.1)	50.9 (1.5)	13.2 (1.3)	3.1 (1.9)	
celecoxib-der2 (i.e., OSU-02067)	this work[b]	−5.6	−64.6 (1.7)	45.1 (1.4)	12.1 (2.0)	−7.3 (1.7)	−6.9
	Zhu et al.[c]	(−49.4)	−71.5 (1.7)	55.6 (1.5)	11.8 (1.5)	−3.7 (1.4)	
celecoxib-der3 (i.e., OSU-03012)	this work[b]	−6.5	−96.8 (2.9)	78.0 (2.8)	12.6 (2.0)	−6.2 (2.0)	−7.2
	Zhu et al.[c]	−4.4	−48.2 (1.9)	45.9 (2.5)	12.1 (0.8)	9.8 (1.4)	

[a] All energies are in kcal/mol. [b] The new binding mode determined in this study. [c] The binding mode reported by Zhu et al.[32] [d] Scores of the molecular docking using the FlexX program. The values in parentheses are scores of the molecular docking using the DOCK program; the DOCK program was used for these binding structures because the molecular docking using the FlexX program did not reveal these binding structures. We note that the DOCK score is the gas phase interaction energy, which does not account for the solvation. Thus, the two types of docking scores cannot be compared. [e] The MM−PBSA calculations were performed on 100 snapshots along a stable MD trajectory for each PDK1−inhibitor binding mode. The results given in the table are the average values calculated for the 100 snapshots. The values in the parentheses are the root-mean-square fluctuations of the calculated energies. [f] Experimental binding free energies are calculated from IC_{50}[32] via $\Delta G_{bind} = RT \ln K_d \approx RT \ln IC_{50}$.

Zhu et al.[32] A remarkable feature of this binding mode is that the 4-methylphenyl group of celecoxib (or the phenanthrene ring of the celecoxib derivatives) is positioned in the ATP sugar/phosphate binding region formed by Gly89, Glu90, Gly91, and Ser94 residues. This hydrophilic environment looks more appropriate to accommodate a hydrophilic functional group of a ligand. The only hydrophobic residue nearby the 4-methylphenyl group of celecoxib is Val96 at a distance >3.5 Å.

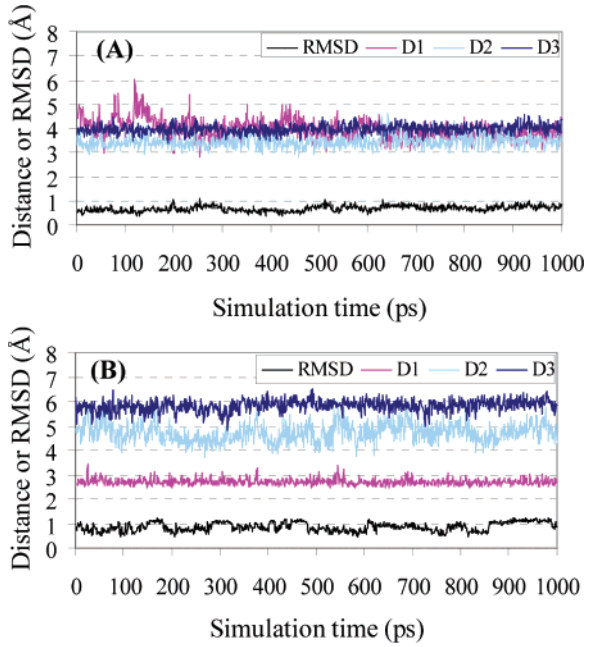

Figure 5. Plots of MD-simulated internuclear distances and root-mean-square deviation (RMSD) for atomic positions of the ligand versus simulation time for PDK1 binding with celecoxib-der1 (see Figure 1 for the structure). (A) The new binding mode determined in this work for the first time: D1 refers to the distance between N1 atom of celecoxib-der1 and one of the two oxygen atoms of Asp223 side chain carboxyl group, D2 is the distance between N4 atom of celecoxib-der1 and the nitrogen atom of Lys111 side chain, and D3 is the distance between N4 atom of celecoxib-der1 and the nitrogen atom of Asp223 backbone. (B) The binding mode similar to that proposed by Zhu et al.:[32] D1 refers to the distance between O1 atom of celecoxib-der1 and the hydroxyl oxygen of Thr222 side chain, D2 is the distance between N1 atom of celecoxib-der1 and the carbonyl oxygen of Ser160 backbone, and D3 is the distance between N4 atom of celecoxib-der1 and the nitrogen atom of Glu166 backbone.

Glu166 is close to both the pyrazole ring and the 4-methylphenyl of celecoxib. The other binding mode (see mode "A" depicted in Figure 6) found in our docking and MD simulations for the first time is totally different. In this newly found binding mode, the 4-methylphenyl moiety of celecoxib stays in the adenine pocket and is sandwiched between the hydrophobic residues Val96 and Leu212, the sulfonamide moiety extends into the sugar/phosphate pocket and forms a hydrogen bond with the carbonyl oxygen of Glu209 backbone, and a nitrogen on the pyrazole ring forms a hydrogen bond with the protonated amine group on the Lys111 side chain. This binding mode allows the CF_3 group to stay in a small hydrophobic pocket defined by residues Leu159, Phe157, Leu113, Met134, and Val143. The

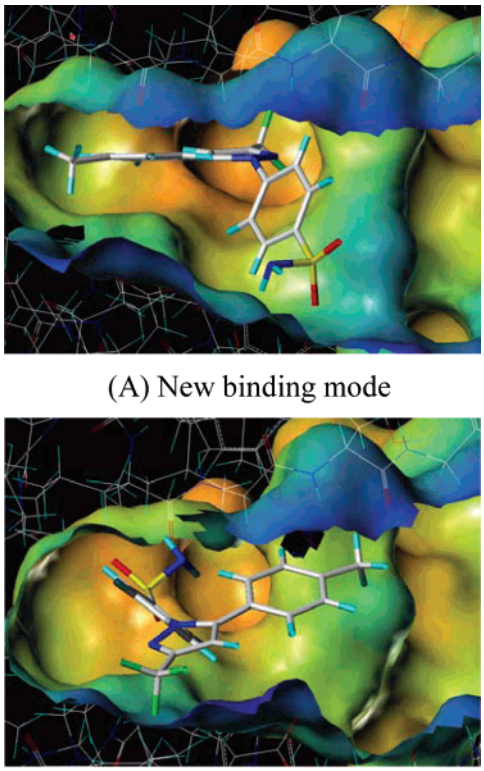

Figure 6. MD-simulated structures of PDK1 binding with celecoxib: (A) new binding mode determined in this work for the first time; (B) binding mode similar to that proposed by Zhu et al.[32]

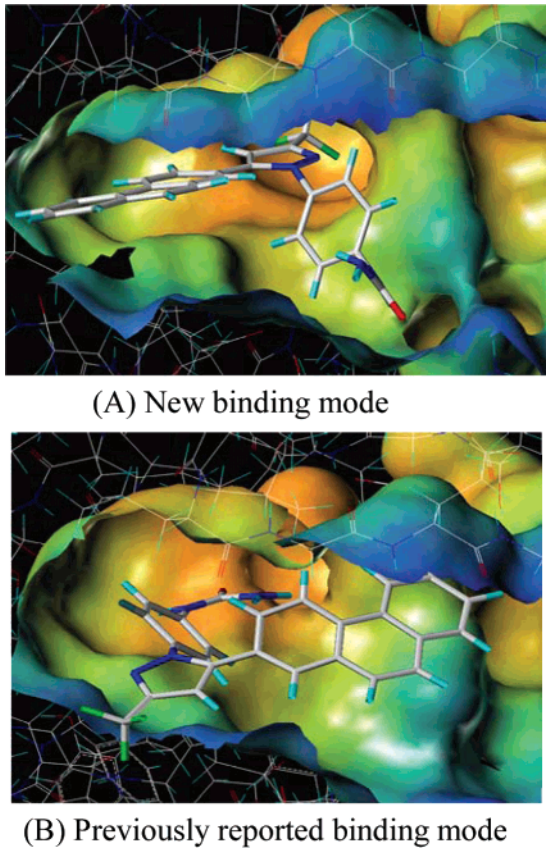

Figure 7. MD-simulated structures of PDK1 binding with celecoxib-der1: (A) new binding mode determined in this work for the first time; (B) binding mode similar to that proposed by Zhu et al.[32]

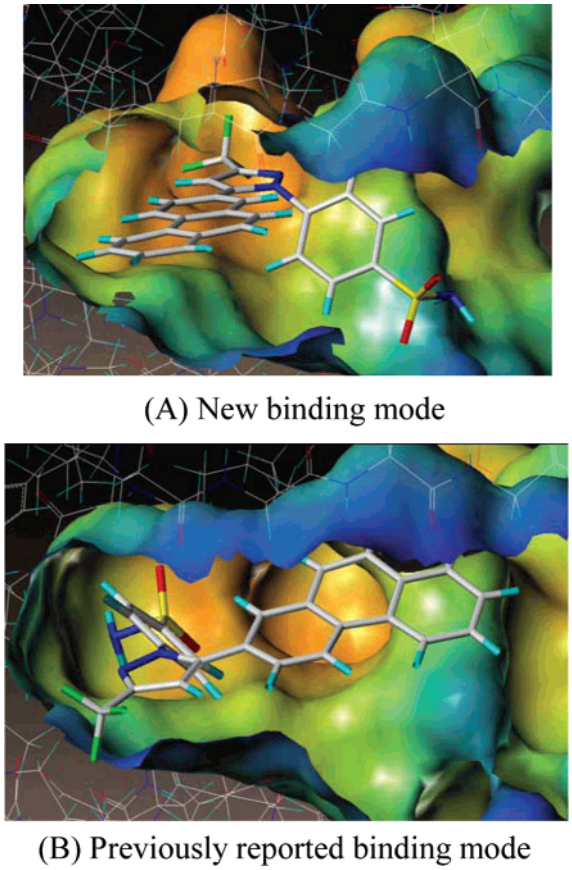

Figure 8. MD-simulated structures of PDK1 binding with celecoxib-der2: (A) new binding mode determined in this work for the first time; (B) binding mode similar to that proposed by Zhu et al.[32]

conserved residues Lys111 and Glu130 are nearby this small pocket. Further, all the celecoxib derivatives examined in this study bind with PDK1 in a way similar to that of celecoxib, as seen in Figures 6−9. For example, when the 4-methylphenyl group of celecoxib is replaced by a phenanthrene ring, celecoxib becomes celecoxib-der2 (see Figure 1) and the phenanthrene ring of celecoxib-der2 also stays in the adenine pocket although the phenanthrene ring is surrounded by more hydrophobic residues (including Leu88 in addition to Val96 and Leu212). An interesting difference is that the terminal sulfonamide group of this derivative forms a hydrogen bond with Asp223, instead of Glu209, for the binding with celecoxib. Celecoxib-der1 and celecoxib-der3 retain the same hydrophobic interactions between the phenanthrene ring and the adenine pocket as that found in celecoxib-der2 binding with PDK1. These derivatives show flexibility in their interactions with the sugar/phosphate pocket. The amino group of celecoxib-der3 forms a hydrogen bond with the carbonyl oxygen of the Glu90 backbone, whereas celecoxib-der1 does not have such a strong hydrogen bond with PDK1.

MM−PBSA calculations were performed to calculate the binding free energies for all of the MD-simulated binding structures, and the calculated binding free energies are summarized in Table 2. We note that the binding free energy for a given binding mode is determined by all of the contributions from the protein−ligand interactions in the gas phase, solvation/desolvation effects, and entropy change. In a comparison between the two different modes of PDK1 binding with a given ligand (i.e., celecoxib or its derivative), one binding mode might be much more favorable than the other in the gas phase, but the solvation/desolvation effects could make a big difference in changing the relative binding free energies. As seen in Table 2, for each of these compounds binding with PDK1, the binding free energy calculated for our newly found binding mode is always significantly lower than that calculated for the other binding mode (similar to that proposed by Zhu et al.[32]), which suggests that our newly found binding mode is significantly more favorable. According to the new binding mode, the binding free energies calculated for PDK1 binding with all of these compounds are reasonably close to the corresponding experimental binding free energies (derived from the experimental IC_{50} values reported by Zhu et al.[32]); the average absolute deviation is ~0.9 kcal/mol. This agreement further supports that the new binding mode found for PDK1 binding with celecoxib and its derivatives in this study is more reasonable.

Further, the new, more favorable binding mode found in this study can aid in better understanding the substituent effects of the celecoxib derivatives on the previously reported biological activity.[32,48] For example, some experimental trends can be understood easily now when we know that the 4-methylphenyl group of celecoxib stays in the hydrophobic adenine pocket. When the 4-methylphenyl group of celecoxib is replaced by a phenanthrene group, celecoxib becomes celecoxib-der2 and the IC_{50} value changes from 48 μM to 9 μM.[32] The activity increase from celecoxib to celecoxib-der2 is attributed to the increase of the size of the hydrophobic functional group (from the 4-methylphenyl to phenanthrene) interacting with the hydrophobic adenine pocket of PDK1. Thus, the hydrophobic interaction for PDK1 binding with celecoxib-der2 should be stronger than that with celecoxib. When the 4-methylphenyl group of celecoxib is replaced by a 4-aminophenyl group, the hydrophobic interaction is expected to decrease and, therefore, its binding affinity with PDK1 is expected to decrease, which

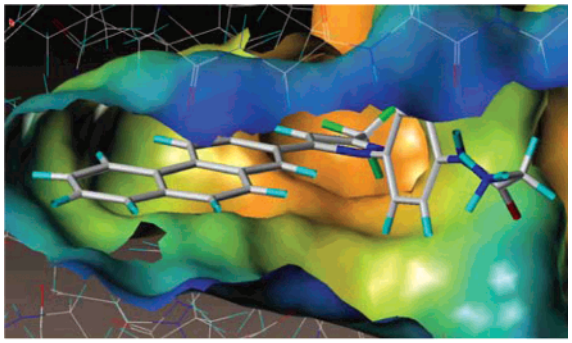

(A) New binding mode

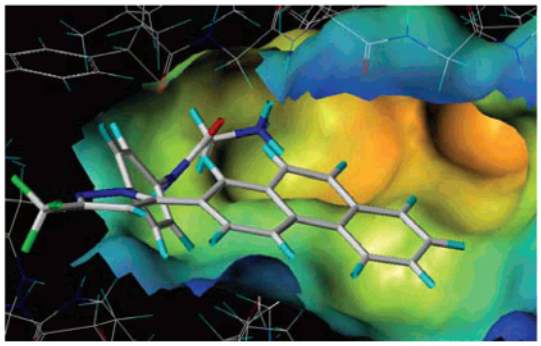

(B) Previously reported binding mode

Figure 9. MD-simulated structures of PDK1 binding with celecoxib-der3: (A) new binding mode determined in this work for the first time; (B) binding mode similar to that proposed by Zhu et al.[32]

is consistent with the experimental observation of the decrease in the apoptotic activity.[48] The molecular structures of celecoxib-der1 and celecoxib-der3 differ by only a $-CH_2-$ group, but show a significant difference in the IC_{50} value (40 μM for celecoxib-der1 versus 5 μM for celecoxib-der3), as seen in Figure 1. According to our newly found binding mode, the amino group of celecoxib-der3 forms a hydrogen bond with the carbonyl oxygen of the Glu90 backbone, whereas similar hydrogen bonding does not exist in celecoxib-der1 binding with PDK1. The difference in the hydrogen bonding reveals that celecoxib-der3 binds with PDK1 more strongly than celecoxib-der1 binds with PDK1, which explains why the IC_{50} value of celecoxib-der3 is significantly lower than that of celecoxib-der1.

Conclusion

Extensive molecular docking and combined molecular dynamics (MD) simulations and molecular mechanics/Poisson−Boltzmann surface area (MM−PBSA) binding free energy calculations have demonstrated a new, more favorable microscopic binding mode concerning how celecoxib and its derivatives bind with 3-phosphoinositide-dependent protein kinase-1 (PDK1), an attractive new target for anticancer therapeutics. The new binding mode is remarkably different from that proposed previously based on simple molecular docking tests. For example, the 4-methylphenyl moiety of celecoxib stays in the hydrophobic adenine pocket and is sandwiched between the hydrophobic residues Val96 and Leu212 according to the new binding mode, whereas the 4-methylphenyl moiety is positioned in the ATP sugar/phosphate binding region (which is hydrophilic) according to the previously proposed binding mode. For celecoxib and all of the derivatives binding with PDK1, the binding free energies determined for the new binding mode by the combined MD simulations and MM−PBSA calculations are always significantly lower than those determined for the previously proposed binding mode. Thus, the new binding is energetically more favorable.

For all of the representative PDK1 inhibitors examined in this study, based on the most favorable binding modes, the calculated binding free energies are all in good agreement with the corresponding experimental activity data. All of the computational results reported in this study strongly suggest that (1) the new microscopic binding mode determined in this work is reliable; (2) the determined new, more favorable binding mode can aid in better understanding the substituent effects of the celecoxib derivatives on the previously reported biological activity data; and (3) the computational protocol tested in this study, i.e., the molecular docking followed by the combined MD simulations and MM−PBSA calculations, is reliable and accurate for predicting protein−ligand binding structures and binding free energies, whereas only performing simple molecular docking could lead to a wrong binding mode and thus mislead the drug design. These new insights will be valuable not only for future rational design of novel, more potent PDK1-specific inhibitors as promising anticancer therapeutics, but also for rational design of drugs targeting other proteins.

Acknowledgment. The research was supported in part by NIH (Grant R01DA013930 to C.-G.Z.) and by the Center for Computational Sciences (CCS) at the University of Kentucky. The authors also acknowledge the CCS for supercomputing time on Superdome.

Supporting Information Available: Three figures showing the trajectories of the molecular dynamics simulations on PDK1 binding with celecoxib and other two derivatives (celecoxib-der2 and celecoxib-der3). This material is available free of charge via the Internet at http://pubs.acs.org.

References and Notes

(1) Fabian, M. A.; Biggs, W. H., III; Treiber, D. K.; Atteridge, C. E.; Azimioara, M. D.; Benedetti, M. G.; Carter, T. A.; Ciceri, P.; Edeen, P. T.; Floyd, M.; Ford, J. M.; Galvin, M.; Gerlach, J. L.; Gortzfeld, R. M.; Herrgard, S.; Insko, D. E.; Insko, M. A.; Lai, A. G.; Lelias, J.-M.; Mehta, S. A.; Milanov, Z. V.; Velasco, A. M.; Wodicka, L. M.; Patel, H. K.; Zarrinkar, P. P.; Lockhart, D. J. *Nat. Biotechnol.* **2005**, *23*, 329−336.

(2) Bianco, R.; Melisi, D.; Ciardiello, F.; Tortora, G. *Eur. J. Cancer* **2006**, *42*, 290−294.

(3) Luo, J.; Manning, B. D.; Cantley, L. C. *Cancer Cell* **2003**, *4*, 257−262.

(4) Hennessy, B. T.; Smith, D. L.; Ram, P. T.; Lu, Y.; Mills, G. B. *Nat. Rev. Drug Discovery* **2005**, *4*, 988−1004.

(5) Bader, A. G.; Kang, S.; Zhao, L.; Vogt, P. K. *Nat. Rev. Cancer* **2005**, *5*, 921−929.

(6) Vara, J. A. F.; Casado, E.; Castro, J. D.; Cejas, P.; Belda-Iniesta, C.; Gonzalez-Baron, M. *Cancer Treat. Rev.* **2004**, *30*, 193−204.

(7) Toker, A.; Newton. A. C. *Cell* **2000**, *103*, 185−188.

(8) Fujita, N.; Tsuruo, T. *Cancer Chemother. Pharmacol.* **2003**, *52*, S24−S28.

(9) Vanhaesebroeck, B.; Alessi, D. R. *Biochem. J.* **2000**, *346*, 561−576.

(10) Alessi, D. R.; Deak, M.; Casamayor, A.; Caudwell, F. B.; Morrice, N.; Norman, D. G.; Gaffney, P.; Reese, C. B.; MacDougall, C. N.; Harbison, D.; Ashworth, A.; Bownes, M. *Curr. Biol.* **1997**, *7*, 776−789.

(11) Currie, R. A.; Walker, K. S.; Gray, A.; Deak, M.; Casamayor, A.; Downes, C. P.; Cohen, P.; Alessi, D. R.; Lucocq, J. *Biochem. J.* **1999**, *337*, 575−583.

(12) Mora, A.; Komander, D.; van Aalten, D. M. F.; Alessi, D. R. *Semin. Cell. Dev. Biol.* **2004**, *15*, 161−170.

(13) Komander, D.; Kular, G.; Deak, M.; Alessi, D. R.; VanAalten, D. M. F. *J. Biol. Chem.* **2005**, *280*, 18797−18802.

(14) Alessi, D. R.; James, S. R.; Downes, C. P.; Holmes, A. B.; Gaffney, P. R. J.; Reese, C. B.; Cohen, P. *Curr. Biol.* **1997**, *7*, 261−269.

(15) Brazil, D. P.; Hemmings, B. A. *Trends Biochem. Sci.* **2001**, *26*, 657−664.

(16) Pullen, N.; Dennis, P. B.; Andjelkovic, M.; Dufner, A.; Kozma, S. C.; Hemmings, B. A.; Thomas, G. *Science* **1998**, *279*, 707−710.
(17) Perrotti, N.; He, R. A.; Phillips, S. A.; Haft, C. R.; Taylor, S. I. *J. Biol. Chem.* **2001**, *276*, 9406−9412.
(18) Newton, A. C. *Biochem. J.* **2003**, *370*, 361−371.
(19) Belham, C.; Wu, S.; Avruch, J. *Curr. Biol.* **1999**, *9*, R93−R96.
(20) Leslie, N. R.; Downes, C. P. *Cell. Signalling* **2002**, *14*, 285−295.
(21) Gao, X.; Yo, P.; Harris, T. K. *Protein Expression Purif.* **2005**, *43*, 44−56.
(22) Kim, D.; Chung, J. *J. Biochem. Mol. Biol.* **2002**, *35*, 106−115.
(23) Sahoo, S.; Brickley, D. R.; Kocherginsky, M.; Conzen, S. D. *Eur. J. Cancer* **2005**, *41*, 2754−2759.
(24) Gao, N.; Flynn, D. C.; Zhang, Z.; Zhong, X. S.; Walker, V.; Liu, K. J.; Shi, X.; Jiang, B. H. *Am. J. Physiol. Cell. Physiol.* **2004**, *287*, C281−C291.
(25) Smith, J. A.; Poteet-Smith, C. E.; Xu, Y.; Errington, T. M.; Hecht, S. M.; Lannignan, D. A. *Cancer Res.* **2005**, *65*, 1027−1034.
(26) Cheng, J. Q.; Lindsley, C. W.; Cheng, G. Z.; Yang, H.; Nicosia, S. V. *Oncogene* **2005**, *24*, 7482−7492.
(27) Zeng, X.; Xu, H.; Glazer. R. I. *Cancer Res.* **2002**, *62*, 3538−3543.
(28) Lin, H-J.; Hsieh, F-C.; Song, H.; Lin, J. *Br. J. Cancer* **2005**, *93*, 1372−1381.
(29) Lawlor, M. A.; Mora, A.; Ashby, P. R.; Williams, M. R.; Murray-Trait, V.; Malone, L.; Prescott, A. R.; Lucocq, J. M.; Alessi, D. R. *EMBO J.* **2002**, *21*, 3728−3738.
(30) Flynn, P.; Wong, M.; Zavar, M.; Dean, N. M.; Stokoe, D. *Curr. Biol.* **2000**, *10*, 1439−1442.
(31) Bayascas, J. R.; Leslie, N. R.; Parsons, R.; Fleming, S., Alessi, D. R. *Curr. Biol.* **2005**, *15*, 1839−1846.
(32) Zhu, J.; Huang, J-W.; Tseng, P-H.; Yang, Y-T.; Fowble, J.; Shiau, C.-W.; Shaw, Y.-J.; Kulp, S. K.; Chen, C.-S. *Cancer Res.* **2004**, *64*, 4309−4318.
(33) Song, X. Q.; Lin, H. P.; Johnson, A. J.; Tseng, P. H.; Yang, Y. T.; Kulp, S. K.; Chen, C.-S. *J. Natl. Cancer Inst.* **2002**, *94*, 585−591.
(34) Kulp, S. K.; Yang, Y. T.; Hung, C. C.; Chen, K. F.; Lai, J. P.; Tseng, P. H.; Fowble, J. W.; Ward, P. J.; Chen, C.-S. *Cancer Res.* **2004**, *64*, 1444−1451.
(35) Carlton, P. S.; Hoot, D. R.; Zhu, J. X.; Chen, C.-S.; Bahnson, R. R.; Clinton, S. K. *Cancer Epidemiol. Biomarkers Prev.* **2004**, *13*, 1877S−1878S.
(36) Feldman, R. I.; Wu, J. M.; Polokoff, M. A.; Kochanny, M. J.; Dinter, H.; Zhu, D.; Biroc, S. L.; Alicke, B.; Bryant, J.; Yuan, S.; Buckman, B. O.; Lentz, D.; Ferrer, M.; Whitlow, M.; Alder, M.; Finster, S.; Chang, Z.; Arnaiz, D. O. *J. Biol. Chem.* **2005**, *280*, 19867−19874.
(37) Lehmann, F. S.; Beglinger, C. *Curr. Top. Med. Chem.* **2005**, *5*, 449−464.
(38) http://www.medicinenet.com/celecoxib/article.htm.
(39) Suganuma, M.; Kurusu, M.; Suzuki, K.; Tasaki, E.; Fujiki, H. *Int. J. Cancer* **2006**, *119*, 33−40.
(40) Reckamp, K. L.; Krysan, K.; Morrow, J. D.; Milne, G. L.; Newman, R. A.; Tucker, C.; Elashoff, R. M.; Dubinett, S. M.; Figlin, R. A. *Clin. Cancer Res.* **2006**, *12*, 3381−3388.
(41) Ferrandina, G.; Ranelletti, F. O.; Legge, F.; Salutari, V.; Martinelli, E.; Fattorossi, A.; Lorusso, D.; Zannoni, G.; Vellone, V.; Pagila, A.; Scambia, G. *Clin. Cancer Res.* **2006**, *12*, 2055−2060.
(42) Zhang, G-S.; Liu, D-S.; Dai, C-W.; Li, R-J. *Am. J. Hematol.* **2006**, *81*, 242−255.
(43) Hahn, T.; Alvarez, I.; Kobie, J. J.; Ramanathapuram, L.; Dial, S.; Fulton, A.; Besselsen, D.; Walker, E.; Akporiaye, E. T. *Int. J. Cancer* **2006**, *118*, 2220−2231.
(44) Klenke, F. M.; Gebhard, M.-M.; Ewerbeck, V.; Abdollahi, A.; Huber, P. E.; Sckell, A. *BMC Cancer* **2006**, *6*, 9.
(45) Pruthi, R. S.; Derksen, J. E.; Moore, D.; Carson, C. C.; Grigson, G.; Watkins, C.; Wallen, E. *Clin. Cancer Res.* **2006**, *12*, 2172−2177.
(46) Harris, R. E.; Beebe-Donk, J.; Alshafie, G. A. *BMC Cancer* **2006**, *6*, 27.
(47) http://www.cancer.gov/newscenter/COXInhibitorsFactSheet.
(48) Zhu, J.; Song, X.; Lin, H-P.; Young, D. C.; Yan, S.; Marquez, V. E.; Chen, C.-S. *J. Natl. Cancer Inst.* **2002**, *94*, 1745−1757.
(49) Arico, S.; Pattingre, S.; Bauvy, C.; Gane, P.; Barbat, A.; Codogno, P.; Ogier-Denis, E. *J. Biol. Chem.* **2002**, *277*, 27613−27621.
(50) Biondi, R. M.; Komander, D.; Thomas, C. C.; Lizcano, J. M.; Deak, M.; Alessi, D. R.; VanAalten, D. M. F. *EMBO J.* **2002**, *21*, 4219−4228.
(51) Komander, D.; Kular, G. S.; Schuttelkopf, A. W.; Prakash, K. R. C.; Bain, J.; Elliott, M.; Garrido-Franco, M.; Kozikowski, A. P.; Alessi, D. R.; VanAalten, D. M. F. *Structure* **2004**, *12*, 215−226.
(52) Komander, D.; Kular, G. S.; Bain, J.; Elliott, M.; Alessi, D. R.; Van Aalten, D. M. F. *Biochem. J.* **2003**, *375*, 255−262.
(53) Vulpetti, A.; Bosotti, R. *Farmaco* **2004**, *59*, 759−765.
(54) Fabbro, D.; Ruetz, S.; Buchdunger, E.; Cowan-Jacob, S. W.; Fendrich, G.; Liebetanz, J.; Mestan, J.; O'Reilly, T.; Traxler, P.; Chaudhuri, B.; Fretz, H.; Zimmermann, J.; Meyer, T.; Caravatti, G.; Furet, P.; Manley, P. W. *Pharmacol. Ther.* **2002**, *93*, 79−98.
(55) Kallblad, P.; Mancera, R. L.; Todorov, N. P. *J. Med. Chem.* **2004**, *47*, 3334−3337.
(56) Kollman, P. A.; Massova, I.; Reyes, C.; Kuhn, B.; Huo, S.; Chong, L.; Lee, M.; Lee, T.; Duan, Y.; Wang, W.; Donini, O.; Cieplak, P.; Srinivasan, J.; Case, D. A.; Cheatham, T. E. *Acc. Chem. Res.* **2000**, *33*, 889−897.
(57) Wang, J.; Kang, X.; Kuntz, I. D.; Kollman, P. A. *J. Med. Chem.* **2005**, *48*, 2432−2444.
(58) Hamza, A.; Zhan, C.-G. *J. Phys. Chem. B* **2006**, *110*, 2910−2917.
(59) Berman, H. M.; Westbrook, J.; Feng, Z.; Gilliland, G.; Bhat, T. N.; Weissig, H.; Shindyalov, I. N.; Bourne, P. E. *Nucleic Acids Res.* **2000**, *28*, 235−242.
(60) Tripos Associates, Inc., 1699 S. Hanley, St. Louis, MO 63144.
(61) Rarey, M.; Kramer, B.; Lengauer, T.; Kleb, G. *J. Mol. Biol.* **1996**, *261*, 470−489.
(62) Rarey, M.; Wefing, S.; Lengauer, T. *J. Comput.-Aided Mol. Des.* **1996**, *10*, 41−54.
(63) Clark, M.; Cramer, R. D., III; Van Opdenhosch, N. *J. Comput. Chem.* **1989**, *10*, 982−1012.
(64) Shoichet, B. K.; Kuntz, I. D.; Bodian, D. L. *J. Comput. Chem.* **1992**, *13*, 380−397.
(65) Meng, E. C.; Shoichet, B. K.; Kuntz, I. D. *J. Comput. Chem.* **1992**, *13*, 505−524.
(66) Meng, E. C.; Gschwend, D. A.; Blaney, J. M.; Kuntz, I. D. *Proteins: Struct. Funct. Genet.* **1993**, *17*, 268−278.
(67) Ewing, T. J. A.; Makino, S.; Skillman, A. G.; Kuntz, I. D. *J. Comput.-Aided Mol. Des.* **2001**, *15*, 411−428.
(68) Bohm, H. J. *J. Comput.-Aided Mol. Des.* **1994**, *8*, 243−256.
(69) Klebe, G. *J. Mol. Biol.* **1994**, *237*, 212−235.
(70) Knegtel, R. M. A.; Bayada, D. M.; Engh, R. A.; Saal, W. V. D.; Geerestein, J. V.; Grootenhius, D. J. *J. Comput.-Aided Mol. Des.* **1999**, *13*, 167−183.
(71) Desjarlais, R. L.; Sheridan, R. P.; Seibel, G. L.; Dixon, J. S.; Kuntz, I. D.; Venkataraghavan, R. *J. Med. Chem.* **1988**, *31*, 722−729.
(72) (a) Zhan, C.-G.; Zheng, F.; Landry, D. W. *J. Am. Chem. Soc.* **2003**, *125*, 2462−2474. (b) Pan, Y.; Gao, D.; Yang, W.; Cho, H.; Yang, G.; Tai, H.-H.; Zhan, C.-G. *Proc. Natl. Acad. Sci. U.S.A.* **2005**, *102*, 16656−16661. (c) Zhan, C.-G.; Gao, D. *Biophys. J.* **2005**, *89*, 3863−3872. (d) Gao, D.; Zhan, C.-G. *J. Phys. Chem. B* **2005**, *109*, 23070−23076. (e) Gao, D.; Zhan, C.-G. *Proteins* **2006**, *62*, 99−110. (f) Gao, D.; Cho, H.; Yang, W.; Pan, Y.; Yang, G.-F.; Tai, H.-H.; Zhan, C.-G. *Angew. Chem., Int. Ed.* **2006**, *45*, 653−657.
(73) (a) Hamza, A.; Cho, H.; Tai, H.-H.; Zhan, C.-G. *J. Phys. Chem. B* **2005**, *109*, 4776−4782. (b) Hamza, A.; Cho, H.; Tai, H.-H.; Zhan, C.-G. *Bioorg. Med. Chem.* **2005**, *13*, 4544−4551.
(74) (a) Zhan, C.-G.; Norberto de Souza, O.; Rittenhouse, R.; Ornstein, R. L. *J. Am. Chem. Soc.* **1999**, *121*, 7279−7282. (b) Koca, J.; Zhan, C.-G.; Rittenhouse, R.; Ornstein, R. L. *J. Am. Chem. Soc.* **2001**, *123*, 817−826. (c) Koca, J.; Zhan, C.-G.; Rittenhouse, R. C.; Ornstein, R. L. *J. Comput. Chem.* **2003**, *24*, 368−378.
(75) Case, D. A.; Darden, T. A.; Cheatham, T. E., III; Simmerling, C. L.; Wang, J.; Duke, R. E.; Luo, R.; Merz, K. M.; Wang, B.; Pearlman, D. A.; Crowley, M.; Brozell, S.; Tsui, V.; Gohlke, H.; Mongan, J.; Hornak, V.; Cui, G.; Beroza, P.; Schafmeister, C.; Caldwell, J. W.; Ross, W. S.; Kollman, P. A. *AMBER 8*; University of California: San Francisco, 2004.
(76) Bayly, C. I.; Cieplak, P.; Cornell, W. D.; Kollman, P. A. *J. Phys. Chem.* **1993**, *97*, 10269−10280.
(77) Frisch, M. J.; Trucks, G. W.; Schlegel, H. B.; Scuseria, G. E.; Robb, M. A.; Cheeseman, J. R.; Montgomery, J. A., Jr.; Verven, T.; Kudin, K. N.; Burant, J. C.; Millam, J. M.; Iyengar, S. S.; Tomasi, J.; Barone, V.; Mennucci, B.; Cossi, M.; Scalmani, G.; Rega, N.; Petersson, G. A.; Nakatsuji, H.; Hada, M.; Ehara, M.; Toyota, K.; Fukuda, R.; Hasegawa, J.; Ishida, M.; Nakajima, T.; Honda, Y.; Kitao, O.; Nakai, H.; Klene, M.; Li, X.; Knox, J. E.; Hratchian, H. P.; Cross, J. B.; Adamo, C.; Jaramillo, J.; Gomperts, R.; Stratmann, R. E.; Yazyev, O.; Austin, A. J.; Cammi, R.; Pomelli, C.; Ochterski, J. W.; Ayala, P. Y.; Morokumo, K.; Voth, G. A.; Salvador, P.; Dannenberg, J. J.; Zakrzewski, V. G.; Dapprich, S.; Daniels, A. D.; Strain, M. C.; Farkas, O.; Malick, D. K.; Rabuck, A. D.; Raghavachari, K.; Foresman, J. B.; Ortiz, J. V.; Cui, Q.; Baboul, A. G.; Clifford, S.; Cioslowski, J.; Stefanov, B. B.; Liu, G.; Liashenko, A.; Piskorz, P.; Komaromi, I.; Martin, R. L.; Fox, D. J.; Keith, T.; Al-Laham, M. A.; Peng, C. Y.; Nanayakkara, A.; Challacombe, M.; Gill, P. M.; Wong, M. W.; Gonzalez, C.; Pople, J. A. *Gaussian 03*, revision A.1; Gaussian, Inc.: Pittsburgh, 2003.
(78) Jorgensen, W. L.; Chandrasekhar, J.; Madura, J. D.; Klein, M. L. J. *J. Chem. Phys.* **1983**, *79*, 926−935.
(79) Berendsen, H. C.; Postma, J. P. M.; van Gunsteren, W. F.; DiNola, A.; Haak, J. R. *J. Chem. Phys.* **1984**, *81*, 3684−3690.
(80) Ryckaert, J. P.; Ciccotti, G.; Berendsen, H. C. *J. Comput. Phys.* **1977**, *23*, 327−341.

(81) Essmann, U.; Perera, L.; Berkowitz, M. L.; Darden, T. A.; Lee, H.; Pedersen, L. G. *J. Chem. Phys.* **1995**, *103*, 8577−8593.

(82) Gilson, M. K.; Sharp, K. A.; Honig, B. H. *J. Comput. Chem.* **1988**, *9*, 327−335.

(83) Jayaram, B.; Sharp, K. A.; Honig, B. H. *Biopolymers* **1989**, *28*, 975−993.

(84) Sitkoff, D.; Sharp, K.; Honig, B. *J. Phys. Chem.* **1994**, *98*, 1978−1988.

(85) Cornell, W.; Cieplak, P.; Bayly, C.; Goud, I.; Merz, K.; Ferguson, D.; Spellmayer, D.; Fox, T.; Caldwell, J.; Kollman, P. A. *J. Am. Chem. Soc.* **1995**, *117*, 5179−5197.

(86) Sanner, M. F.; Olson, A. J.; Spehner, J. C. *Biopolymers* **1996**, *38*, 305−320.

(87) McQuarrie, D. A. A. *Statistical Mechanics*; Harper & Row: New York, 1976.

(88) Brooks, B. R.; Janezic, D.; Karplus, M. *J. Comput. Chem.* **1995**, *16*, 1522−1542.